

Fractional-order model of a non-linear inductor

A.M. LOPES^{1*} and J.A. TENREIRO MACHADO²

¹UISPA–LAETA/INEGI, Faculty of Engineering, University of Porto, Rua Dr. Roberto Frias, 4200–465 Porto, Portugal

²Institute of Engineering, Polytechnic of Porto, Dept. of Electrical Engineering, Rua Dr. António Bernardino de Almeida 431, 4249–015 Porto, Portugal

Abstract. This paper adopts a fractional calculus perspective to describe a non-linear electrical inductor. First, the electrical impedance spectroscopy technique is used for measuring the impedance of the device. Second, the experimental data is approximated by means of fractional-order models. The results demonstrate that the proposed approach represents the inductor using a limited number of parameters, while highlighting its most relevant characteristics.

Key words: fractional-order models, inductor, electrical impedance spectroscopy.

1. Introduction

An ideal inductor is characterized by the impedance $Z(j\omega) = j\omega L$, where $j = \sqrt{-1}$, the parameter L denotes the inductance, $\omega = 2\pi f$ represents the angular frequency and f is the frequency. However, such device has no physical correspondence, since the model ignores the ohmic resistance of the winding, the parasitic capacitance between neighbor turns, the hysteresis and eddy-current losses in the magnetic core, and the skin effect in the wire. Additionally, the nonlinearities are dependent on the amplitude and frequency, being more critical at higher frequencies [1].

Classical models describe a real inductor by means of equivalent electric circuits, where the inductor is associated in series/parallel with resistances and capacitors. However, these models reveal difficulties in describing the nonlinear and the skin effects that characterize many inductors, and their accurate modeling is a challenging exercise [2].

Fractional calculus (FC) generalizes the concepts of standard differential calculus to non-integer orders [3–5]. Recently, FC was adopted for modeling natural and artificial signals and systems characterized by power-law behavior, long range memory effects, non-locality, and fractal properties [6–11], opening new avenues towards the generalization of classical laws, devices and systems [12–18].

In the field of electromagnetism, the tools of FC were applied successfully to describe the behavior of electric machines [19–21] and other devices [12, 22]. Specifically for modeling inductors, Schäfer and Krüger [1, 2] showed that fractional models are suitable for describing hysteresis losses in the inductor core.

In this paper we adopt FC to describe an inductor [23]. The electrical impedance spectroscopy (EIS) technique is used for measuring the equivalent impedance of the device, and the

experimental data is approximated by means of fractional-order (FO) empirical transfer functions. The results demonstrate that FO models represent conveniently the dynamics of the inductor, while requiring a limited number of parameters.

Having these ideas in mind, this paper is organized as follows. Section 2 introduces the main tools adopted in the study of the inductor, namely the concepts of FC, the empirical FC models, and the EIS. Section 3 models the inductor electrical impedance and analyses its behavior. Finally, Section 4 draws the main conclusions.

2. Fundamental Concepts

This section outlines the mathematical tools adopted in the follow-up.

2.1. Fractional Calculus. We can find in the literature several definitions of fractional derivatives and integrals [24]. Researchers use mostly the Riemann-Liouville (RL), the Grünwald-Letnikov (GL) and the Caputo (C):

$${}^{RL}D_t^\alpha f(t) = \frac{1}{\Gamma(n-\alpha)} \frac{d^n}{dt^n} \int_a^t \frac{f(\tau)}{(t-\tau)^{\alpha-n+1}} d\tau, \quad (1)$$

$$n-1 < \alpha < n,$$

$${}^{GL}D_t^\alpha f(t) = \lim_{h \rightarrow 0} h^{-\alpha} \sum_{m=0}^{\lfloor \frac{t-a}{h} \rfloor} (-1)^m \binom{\alpha}{m} f(t-mh), \quad (2)$$

$$\alpha \in \mathbb{R}, \quad \alpha > 0,$$

$${}^C D_t^\alpha f(t) = \frac{1}{\Gamma(n-\alpha)} \int_a^t \frac{f^{(n)}(\tau)}{(t-\tau)^{\alpha-n+1}} d\tau, \quad (3)$$

$$n-1 < \alpha < n, \quad \alpha > 0,$$

*e-mail: aml@fe.up.pt

Manuscript submitted 2017-12-29, revised 2018-02-20, initially accepted for publication 2018-04-14, published in February 2019.

where $\Gamma(\cdot)$ represents the Euler's gamma function, the operator $[\cdot]$ calculates the integer part, h is the time increment and $\{t, a\} \in \mathbb{R}$ ($t > a$) are the upper and lower limits of the interval, respectively.

For a large class of functions, the RL, GL and C formulations can be considered "equivalent" since they lead to identical results [25]. Moreover, since in many practical applications we consider $a = 0$, we often adopt D_t^α to denote the generalized "differintegral" operator.

The Laplace, for zero initial conditions, and the Fourier transforms yield the expressions:

$$\mathcal{L}\{D_t^\alpha f(t)\} = s^\alpha \mathcal{L}\{f(t)\}, \quad (4)$$

$$\mathcal{F}\{D_t^\alpha f(t)\} = (j\omega)^\alpha \mathcal{F}\{f(t)\}, \quad (5)$$

where s denotes the Laplace variable, and \mathcal{L} and \mathcal{F} represent the Laplace and Fourier operators, respectively. These transforms allow the generalization of classical tools, such as the root locus, Bode, Nyquist and state-space methods, to FO systems [26, 27].

The Mittag-Leffler function, $E_\alpha(t)$, is defined by:

$$E_\alpha(t) = \sum_{m=0}^{\infty} \frac{t^m}{\Gamma(\alpha m + 1)}, \quad (6)$$

establishing a relationship between exponential and power law behaviors that occur for integer and fractional dynamics, respectively [9]. Its Laplace transform is given by:

$$\mathcal{L}\{E_\alpha(\pm at^\alpha)\} = \frac{s^{\alpha-1}}{s^\alpha \mp a}. \quad (7)$$

2.2. Empirical FO Models. For an experimental spectrum, we need a model that fits the numerical values, having in mind some parsimony in the total number of parameters [28, 29]. Several empirical models were proposed [30] in the scope of the dielectric relaxation phenomenon. The integer-order Debye (D) model [31] does not describe adequately the response of many materials, since it neglects relaxing effects and long-memory phenomena [32, 33].

The Cole-Cole (CC), Cole-Davidson (CD) and Havriliak-Negami (HN) models generalize the integer-order description [34–36]. These empirical expressions are, in fact, particular cases of FO models [37, 38]. In the Fourier domain, the D, CC, CD and HN are given by the expressions [38]:

$$\tilde{\varepsilon}_D(j\omega) = \frac{\varepsilon^*(j\omega) - \varepsilon_\infty}{\varepsilon_0 - \varepsilon_\infty} = \frac{1}{1 + j\omega\tau}, \quad (8)$$

$$\tilde{\varepsilon}_{CC}(j\omega) = \frac{1}{1 + (j\omega\tau)^\alpha}, \quad (9)$$

$$\tilde{\varepsilon}_{CD}(j\omega) = \frac{1}{(1 + j\omega\tau)^\beta}, \quad (10)$$

$$\tilde{\varepsilon}_{HN}(j\omega) = \frac{1}{[1 + (j\omega\tau)^\alpha]^\beta}, \quad (11)$$

where $0 < \alpha, \beta \leq 1$, $\tilde{\varepsilon}$ is the complex susceptibility, $\{\varepsilon_0, \varepsilon_\infty\}$ are the low and high-frequency limits of the complex dielectric permittivity, ε^* , and τ denotes the relaxation time.

Models (9–11) are ubiquitous in natural and artificial phenomena, and often are denoted as Randles cell, constant phase element, or fractance, and have been under investigation [39, 40]. One open question concerns the units of the parameters involved, but no effective measurement units have been proposed for a fractor. Usually, this is not an issue in real systems as we may use a scaling term to give a result in real integer order units [41, 42].

2.3. Electrical Impedance Spectroscopy. The EIS technique measures the electrical impedance of a specimen object [9, 43]. The EIS is straightforward to implement, avoiding complicated and time consuming procedures. The EIS has been used in the description of vegetable [44, 45] and animal [46, 47] tissues, food liquids [48, 49], materials [50, 51], devices [52, 53], and elements [54, 55].

The EIS starts by applying to the sample electric sinusoidal input signals, and registering the amplitude and phase shift of the output steady-state sinusoidal voltage, $v(t)$, and current, $i(t)$:

$$v(t) = V \cos(\omega t + \theta_V), \quad (12a)$$

$$i(t) = I \cos(\omega t + \theta_I), \quad (12b)$$

where $\{V, I\}$ and $\{\theta_V, \theta_I\}$ are the amplitudes and phase shifts of the voltage and current, respectively.

The signals $v(t)$ and $i(t)$ can be represented in the Fourier domain:

$$\mathbf{V}(j\omega) = V \cdot e^{j\theta_V}, \quad (13a)$$

$$\mathbf{I}(j\omega) = I \cdot e^{j\theta_I}, \quad (13b)$$

where the impedance $\mathbf{Z}(j\omega)$ is given by:

$$\begin{aligned} \mathbf{Z}(j\omega) &= \frac{\mathbf{V}(j\omega)}{\mathbf{I}(j\omega)} = \frac{V}{I} \cdot e^{j(\theta_V - \theta_I)} = \\ &= |\mathbf{Z}(j\omega)| \cdot e^{j\arg[\mathbf{Z}(j\omega)]}. \end{aligned} \quad (14)$$

3. EIS Analysis of an Inductor

Different equipment can be used for measuring impedances in the scope of the EIS. Commercial impedance analyzers are often adopted, since they are easy to use and accurate. They inject an adjustable frequency, constant amplitude, sinusoidal AC current through the sample under test and measure the voltage drop across it.

The main disadvantage of the commercial impedance analyzers is their high cost. Moreover, custom solutions using

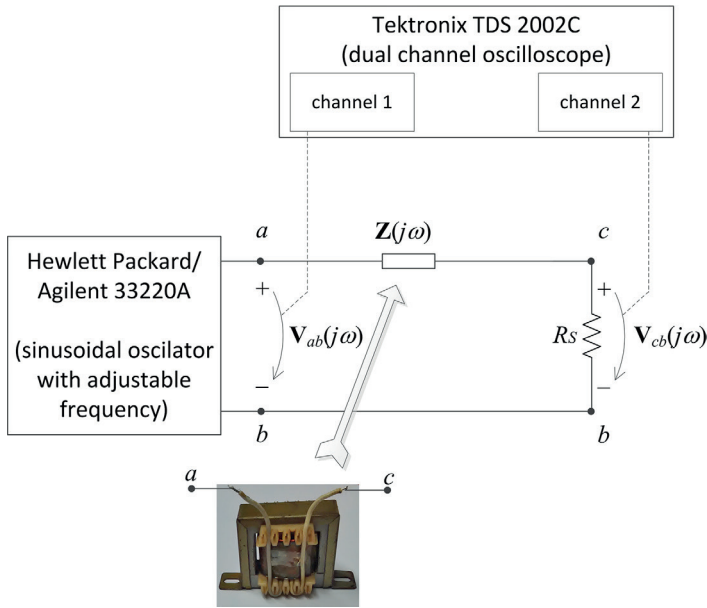


Fig. 1. Experimental set-up EIS for measuring $Z(j\omega)$

general purpose equipment may be advantageous when the specifications of the impedance analyzers are not compatible with the specimens to be studied [56, 57].

The diagram of Fig. 1 shows the experimental set-up adopted herein [9, 43] using general purpose equipment. The inductor is connected in series with an adaptation metal film resistance, $R_s = 27 \Omega$, for achieving good signal/noise ratio, while avoiding interference at high frequencies [58]. A Hewlett Packard/Agilent 33220 A function generator applies a sinusoidal AC voltage with amplitude V_{ab} to the circuit (i.e., the voltage divider) and a Tektronix TDS 2002C two channel oscilloscope measures the voltages V_{ab} and V_{cb} . The oscilloscope bandwidth is 70 MHz, with DC vertical accuracy of $\pm(3\% \times \text{reading} + 0.1 \text{ div} + 1 \text{ mV})$, and delta time accuracy equal to $\pm(1 \text{ sample interval} + 100 \text{ ppm} \times \text{reading} + 0.6 \text{ ns})$.

The tested inductor has a closed iron core, a resistance $R = 0.6 \Omega$, measured by a Keithley 2000 digital multimeter by means of the 4-wire method, and an inductance $L = 11.5 \text{ mH}$, measured with a Escort ELC-131D LCR bridge at the frequency of 120 Hz. The experiments consist of 10 sets of measurements with exciting voltages $V_{ab} = \{1, \dots, 10\} \text{ V}$. For each fixed-amplitude V_{ab} the impedance $Z(j\omega)$ is obtained for the frequency range $2\pi \cdot 10 \leq \omega \leq 2\pi \cdot 10^4 \text{ rad/s}$, at $L = 27$ logarithmically spaced points using the expression:

$$Z(j\omega) = R_s \cdot \left(\frac{V_{ab}(j\omega)}{V_{cb}(j\omega)} - 1 \right), \quad (15)$$

where the signals $v_{ab}(t) = V_{ab} \cos(\omega t)$ and $v_{cb}(t) = V_{cb} \cos(\omega t + \theta)$ are measured directly by the oscilloscope, and θ denotes the phase shift between $v_{cb}(t)$ and $v_{ab}(t)$.

3.1. The Five-parameter Model. The FO models are fitted into the experimental data in order to minimize the Canber-

ra-based distance, J , between the experimental, Z_e , and model, Z_m , impedances:

$$J = \frac{1}{L} \sum_{k=1}^L \cdot \left(\frac{|\text{Re}[Z_e(j\omega_k)] - \text{Re}[Z_m(j\omega_k)]|}{|\text{Re}[Z_e(j\omega_k)]| + |\text{Re}[Z_m(j\omega_k)]|} + \frac{|\text{Im}[Z_e(j\omega_k)] - \text{Im}[Z_m(j\omega_k)]|}{|\text{Im}[Z_e(j\omega_k)]| + |\text{Im}[Z_m(j\omega_k)]|} \right), \quad (16)$$

where $\text{Re}[\cdot]$ and $\text{Im}[\cdot]$ represent the real and imaginary parts.

Expression (16) captures the relative error of the curve fitting. This avoids saturation effects that occur when using the standard Euclidean norm due to the simultaneous presence of large and small values.

A good fit occurs for the 5-parameter model:

$$Z_m(j\omega) = K \cdot \frac{\left(1 + \frac{j\omega}{z}\right)^\beta}{\left(1 + \frac{j\omega}{p}\right)^\alpha}, \quad (17)$$

where $K = R = 0.6$ is the inductor resistance. Expression (17) represents a compromise between model complexity and quality of fitting between experimental and analytical results.

The polar, Nichols and Bode diagrams of the experimental, $Z_e(j\omega)$, and approximating FO model, $Z_m(j\omega)$, are depicted in Fig. 2 for the excitation voltage $V_{ab} = 5 \text{ V}$. The charts reveal the adequacy of expression (17) when modeling the inductor. For the other values of V_{ab} the results are identical.

Table 1 summarizes the values of the parameters and the fitness function obtained for the 10 excitation voltages $V_{ab} = \{1, \dots, 10\} \text{ V}$. Figure 3 depicts the variation of the set of parameters and fit error $\{z, \beta, p, \alpha, J\}$ with V_{ab} . We observe that the parameters decrease for increasing values of the excitation voltage. The fitness function, J , is minimal for intermediate values of V_{ab} , corresponding to a closer fit between $Z_m(j\omega)$ and $Z_e(j\omega)$.

Table 1
 Values of the parameters of the model and the fitness function for $V_{ab} = \{1, \dots, 10\} \text{ V}$

V_{ab}	z	β	p	α	J
1	38.96	0.92	8400	0.60	0.22
2	33.93	0.93	6200	0.55	0.16
3	32.67	0.92	6600	0.54	0.13
4	28.90	0.92	5100	0.54	0.11
5	28.90	0.92	5500	0.54	0.13
6	26.39	0.92	4800	0.54	0.10
7	22.62	0.90	4000	0.52	0.10
8	21.36	0.90	4000	0.52	0.14
9	16.34	0.86	4200	0.51	0.15
10	15.71	0.86	3900	0.50	0.20

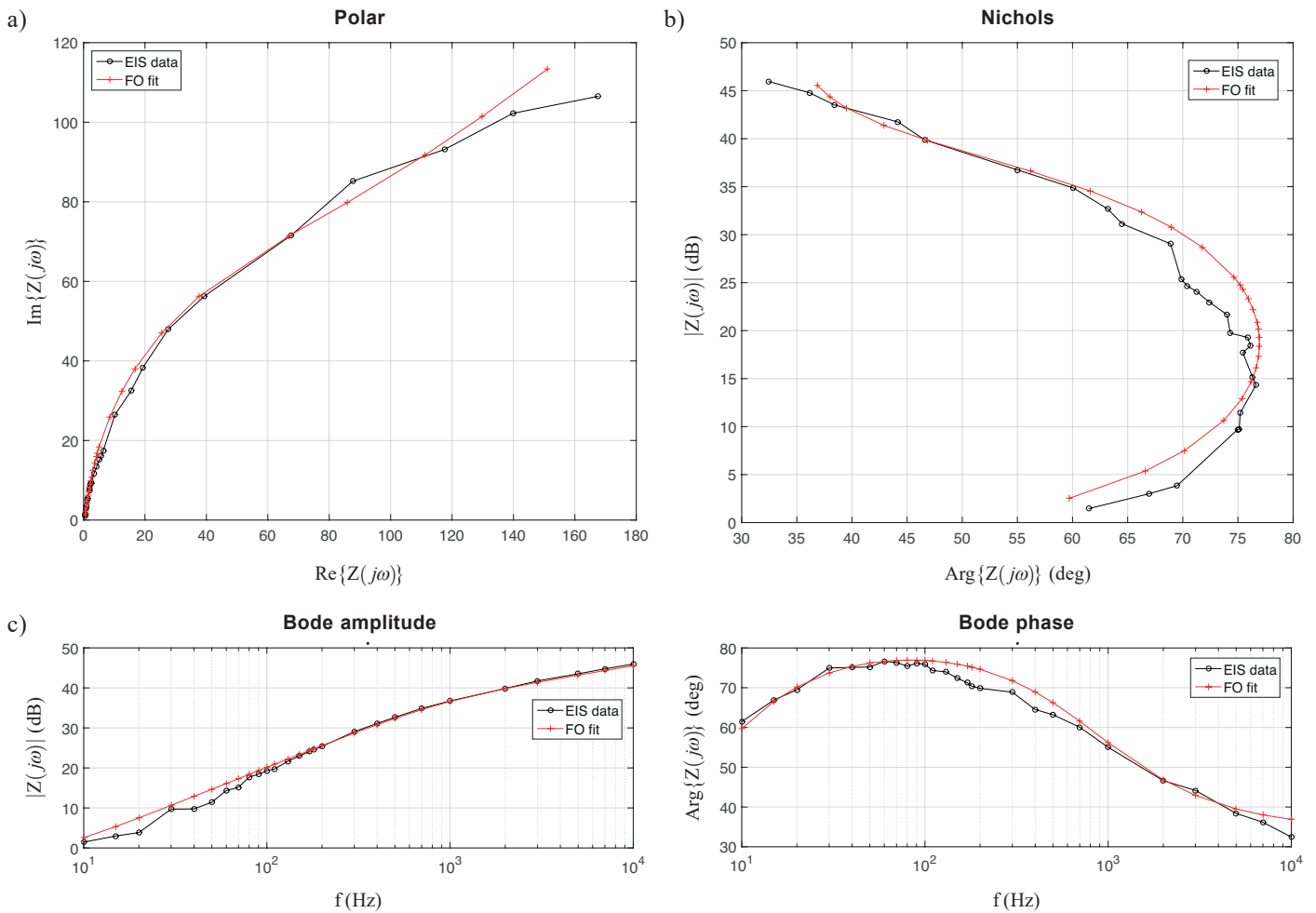


Fig. 2. Diagrams of the experimental and model impedances, $Z_e(j\omega)$ and $Z_m(j\omega)$, of the inductor for $V_{ab} = 5$ V: a) – Polar; b) – Nichols; c) – Bode

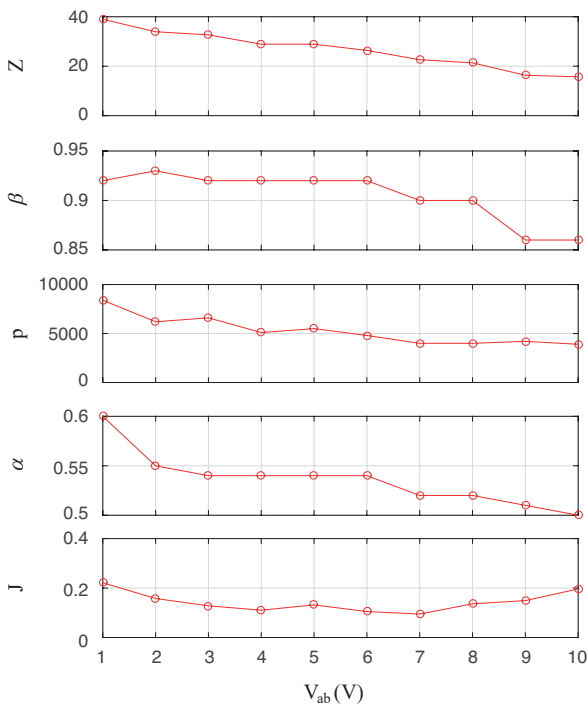


Fig. 3. The variation of $\{z, \beta, p, \alpha, J\}$ with $V_{ab} = \{1, \dots, 10\}$

Figure 4 depicts the Nichols diagrams of the inductor obtained with the experimental impedances, for $V_{ab} = \{1, \dots, 10\}$ V. The points corresponding to the same frequency/ amplitude are also connected [59], so that we have the locus of constant frequency/ amplitude versus variable amplitude/frequency. We observe that the impedance Z_e depends on V_{ab} , reflecting the nonlinear nature of the device. At low frequencies Z_e is more sensitive to the excitation voltage, meaning that the non-linear component represents a larger part of the total value.

The results demonstrate that model (17) yields a quantitative description and reliable characterization of the inductor. Nevertheless, the number of model parameters necessary is high and the adherence between the heuristic model and the experimental data in Fig. 2 is limited.

3.2. The Asymptotic Model. In subsection 3.1 we adopted a model covering all measured spectrum. However, it was observed that the curve fitting was not completely satisfactory at low frequencies. So, the question remains of using a simple model that adjusts adequately the experimental data while describing the main characteristics of the inductor. In this perspective, this subsection tests a model that fits the asymptotic behavior of $Z_e(j\omega)$ at low, mid and high frequencies (to be

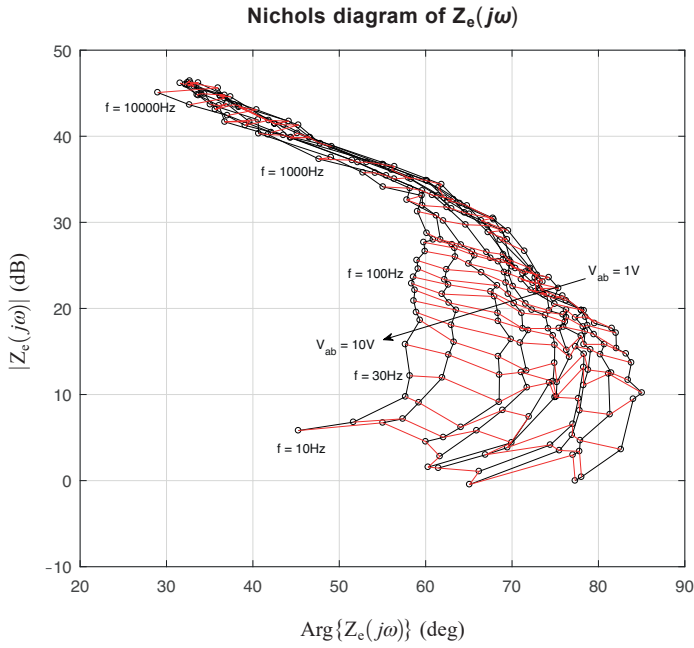


Fig. 4. The Nichols diagrams of the inductor obtained with the experimental impedances, for $V_{ab} = \{1, \dots, 10\}$ V. The black/red lines represent Z_e for constant/variable amplitude V_{ab} versus variable/constant frequency ω

denoted by the subscripts L, M and H). This strategy has the advantages of being simple and requiring a small number of parameters. However, it is not clear what is the “adequate” bandwidth for describing the inductor, and we may overlook some part of the spectrum containing relevant information.

We consider the asymptotic approximation of the experimental data, $Z_e(j\omega)$, by means of the model:

$$\begin{cases} |Z_L(j\omega)| = K = R \\ \arg[Z_L(j\omega)] = 0 \end{cases}, \quad \omega < \omega_L, \quad (18)$$

$$\begin{cases} |Z_M(j\omega)| = K_M \cdot \omega^{\alpha_M} \\ \arg[Z_M(j\omega)] = \frac{\pi}{2} \alpha_M + \theta_M \end{cases}, \quad \omega_L \leq \omega \leq \omega_M, \quad (19)$$

$$\begin{cases} |Z_H(j\omega)| = K_H \cdot \omega^{\alpha_H} \\ \arg[Z_H(j\omega)] = \frac{\pi}{2} \alpha_H \end{cases}, \quad \omega > \omega_H, \quad (20)$$

where $\{\omega_L, \omega_M, \omega_H\}$ are the limit frequencies for calculating the asymptotic approximations. These values were tested manually and therefore at present state their choice is not automatic. The resulting asymptotic model has no physical meaning, in the sense that it does not describe a real-world system. However, expressions (18–20) fit well the experimental data and, as we shall demonstrate, give a reliable description of the measurements.

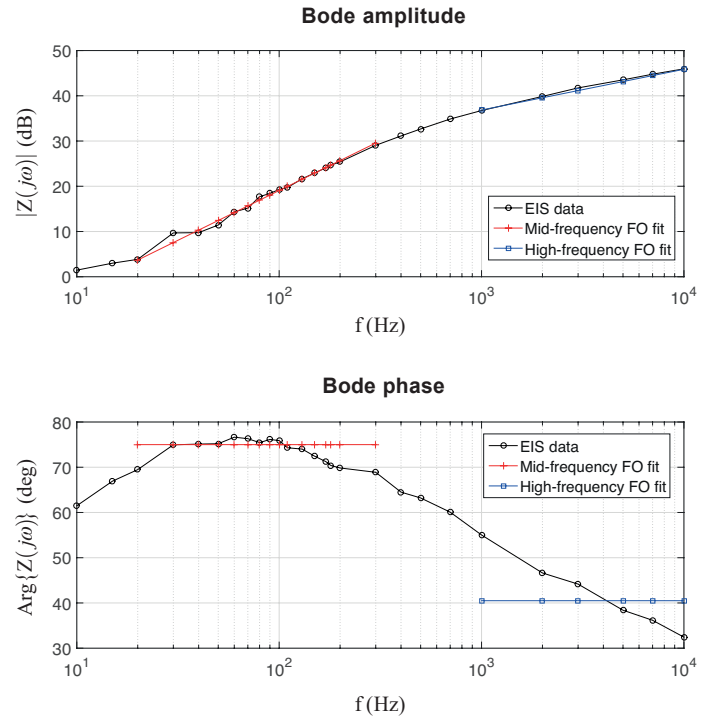


Fig. 5. Bode diagram of the experimental data and the asymptotic model for $V_{ab} = 5$ V and $\{\omega_L, \omega_M, \omega_H\} = \{20, 300, 1000\}$

Figure 5 depicts the Bode diagram of the experimental data and the asymptotic model for $V_{ab} = 5$ V and $\{\omega_L, \omega_M, \omega_H\} = \{20, 300, 1000\}$ Hz. The low-frequency approximation is omitted since the inductor is described by its resistance. For the other excitation voltages the frequency response is similar. Table 2 summarizes the values of the parameters $\{K_M, \alpha_M, \theta_M\}$ and $\{K_H, \alpha_H\}$ obtained for $V_{ab} = \{1, \dots, 10\}$ V. Figure 6 depicts the variation of the two sets. We verify that K_M and θ_M are sensitive to V_{ab} , while the remaining three parameters have limited variations, with particular emphasis to the fractional order α_H that remains constant.

Table 2
 Values of the parameters of the asymptotic model for $V_{ab} = \{1, \dots, 10\}$ V

V_{ab}	K_M	α_M	θ_M	K_H	α_H
1	0.02	0.92	0.00	1.20	0.45
2	0.03	0.89	-0.17	1.30	0.45
3	0.02	0.94	-0.12	1.33	0.45
4	0.03	0.92	-0.09	1.31	0.45
5	0.02	0.97	-0.21	1.36	0.45
6	0.02	0.99	-0.26	1.40	0.45
7	0.03	0.95	-0.26	1.40	0.45
8	0.02	0.99	-0.37	1.40	0.45
9	0.02	0.99	-0.45	1.40	0.45
10	0.03	0.94	-0.44	1.40	0.45

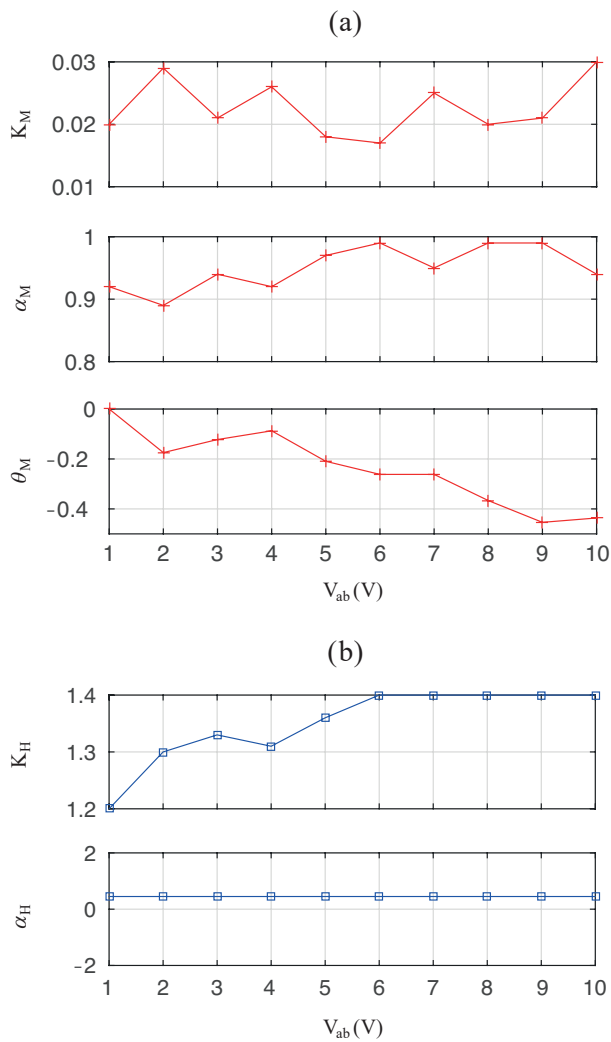


Fig. 6. The variation of the asymptotic model parameters with $V_{ab} = \{1, \dots, 10\}$: a) $\{K_M, \alpha_M, \theta_M\}$; b) $\{K_H, \alpha_H\}$

4. Conclusions

In this paper we used EIS to determine the electrical impedance of an inductor and we adopted FO models to describe the experimental data. We tested both a 5-parameter fractional model and several independent asymptotic expressions. In both cases we observe FO behavior not captured with classical descriptions.

REFERENCES

- [1] I. Schäfer and K. Krüger, Modelling of coils using fractional derivatives, *Journal of Magnetism and Magnetic Materials* 307 (1) (2006) 91–98.
- [2] I. Schäfer and K. Krüger, Modelling of lossy coils using fractional derivatives, *Journal of Physics D: Applied Physics* 41 (4) (2008) 045001.
- [3] D. Baleanu, K. Diethelm, E. Scalas, and J.J. Trujillo, *Models and Numerical Methods*, Vol. 3, World Scientific, 2012.
- [4] C.M. Ionescu, *The human respiratory system: an analysis of the interplay between anatomy, structure, breathing and fractal dynamics*, Springer Science & Business Media, 2013.
- [5] J.T. Machado and A.M. Lopes, The persistence of memory, *Nonlinear Dynamics* 79 (1) (2015) 63–82.
- [6] X.J. Yang, D. Baleanu, and H.M. Srivastava, *Local fractional integral transforms and their applications*, Academic Press, 2015.
- [7] X.-J. Yang and D. Baleanu, Fractal heat conduction problem solved by local fractional variation iteration method, *Thermal Science* 17 (2) (2013) 625–628.
- [8] V.E. Tarasov, Review of some promising fractional physical models, *International Journal of Modern Physics B* 27 (09) (2013) 1330005.
- [9] A.M. Lopes and J.T. Machado, Fractional order models of leaves, *Journal of Vibration and Control* 20 (7) (2014) 998–1008.
- [10] C.I. Muresan, C. Ionescu, S. Folea, and R. De Keyser, Fractional order control of unstable processes: the magnetic levitation study case, *Nonlinear Dynamics* 80 (4) (2015) 1761–1772.
- [11] C. Ionescu and C. Muresan, Sliding mode control for a class of sub-systems with fractional order varying trajectory dynamics, *Fractional Calculus and Applied Analysis* 18 (6) (2015) 1441–1451.
- [12] J.T. Machado and A.M. Galhano, Generalized two-port elements, *Communications in Nonlinear Science and Numerical Simulation* 42 (2017) 451–455.
- [13] J. Machado, A. Lopes, F. Duarte, M. Ortigueira, and R. Rato, Rhapsody in fractional, *Fractional Calculus and Applied Analysis* 17 (4) (2014) 1188–1214.
- [14] M. Lewandowski and M. Orzylowski, Fractional-order models: The case study of the supercapacitor capacitance measurement, *Bull. Pol. Ac.: Tech.* 65 (4) (2017) 449–457.
- [15] D. Mozyrska and E. Pawluszewicz, Local controllability of nonlinear discrete-time fractional order systems, *Bull. Pol. Ac.: Tech.* 61 (1) (2013) 251–256.
- [16] M. Buśłowicz, Stability analysis of continuous-time linear systems consisting of n subsystems with different fractional orders, *Bull. Pol. Ac.: Tech.* 60 (2) (2012) 279–284.
- [17] M.S. Krishna, S. Das, K. Biswas, and B. Goswami, Fabrication of a fractional order capacitor with desired specifications: a study on process identification and characterization, *IEEE Transactions on Electron Devices* 58 (11) (2011) 4067–4073.
- [18] A. Buscarino, R. Caponetto, G. Di Pasquale, L. Fortuna, S. Graziani, and A. Pollicino, Carbon black based capacitive fractional order element towards a new electronic device, *AEU International Journal of Electronics and Communications* 84 (2018) 307–312.
- [19] S. Racewicz, Identification and non-integer order modelling of synchronous machines operating as generator, *Acta Energetica*.
- [20] S. Canat, and J. Faucher, Fractional order: frequential parametric identification of the skin effect in the rotor bar of squirrel cage induction machine, in: *ASME Design Engineering Technical Conferences 2003VIB-48393*, Vol. 48393, 2003.
- [21] A. Jalloul, J.-C. Trigeassou, K. Jelassi, and P. Melchior, Fractional order modeling of rotor skin effect in induction machines, *Nonlinear Dynamics* 73 (1–2) (2013) 801–813.
- [22] J.T. Machado, I.S. Jesus, A. Galhano, and J.B. Cunha, Fractional order electromagnetics, *Signal Processing* 86 (10) (2006) 2637–2644.
- [23] A. Lopes and J. Tenreiro Machado, Fractional-order model of a transformer, in: *FSS2017 – International Symposium on Fractional Signals and Systems*, 2017.

- [24] J.T. Machado, V. Kiryakova, and F. Mainardi, Recent history of fractional calculus, *Communications in Nonlinear Science and Numerical Simulation* 16 (3) (2011) 1140–1153.
- [25] I. Podlubny, Fractional differential equations: an introduction to fractional derivatives, fractional differential equations, to methods of their solution and some of their applications, Vol. 198, Academic press, 1998.
- [26] F. Merrikh-Bayat and M. Afshar, Extending the root-locus method to fractional-order systems, *Journal of Applied Mathematics* 2008.
- [27] I. Petras, Fractional-order nonlinear systems: modeling, analysis and simulation, *Springer Science & Business Media*, 2011.
- [28] B. Maundy, A. Elwakil, and A. Allagui, Extracting the parameters of the single-dispersion Cole bioimpedance model using a magnitude-only method, *Computers and Electronics in Agriculture* 119 (2015) 153–157.
- [29] W. Kuang and S. Nelson, Dielectric relaxation characteristics of fresh fruits and vegetables from 3 to 20 GHz, *Journal of Microwave Power and Electromagnetic Energy* 32 (2) (1997) 115–123.
- [30] T.J. Freeborn, A survey of fractional-order circuit models for biology and biomedicine, *IEEE Journal on Emerging and Selected Topics in Circuits and Systems* 3 (3) (2013) 416–424.
- [31] P.J.W. Debye, Polar molecules, *Chemical Catalog Company*, Incorporated, 1929.
- [32] Y. Feldman, A. Puzenko, and Y. Ryabov, Non-Debye dielectric relaxation in complex materials, *Chemical Physics* 284 (1) (2002) 139–168.
- [33] Z. Vosika, M. Lazarević, J. Simic-Krstić, and D. Koruga, Modeling of bioimpedance for human skin based on fractional distributed order modified Cole model, *FME Transactions* 42 (1) (2014) 74–81.
- [34] K.S. Cole and R.H. Cole, Dispersion and absorption in dielectrics I. Alternating current characteristics, *The Journal of Chemical Physics* 9 (4) (1941) 341–351.
- [35] D. Davidson and R. Cole, Dielectric relaxation in glycerol, propylene glycol, and n-propanol, *The Journal of Chemical Physics* 19 (12) (1951) 1484–1490.
- [36] S. Havriliak and S. Negami, A complex plane analysis of a-dispersions in some polymer systems, in: *Journal of Polymer Science Part C: Polymer Symposia*, Vol. 14, Wiley Online Library, 1966, pp. 99–117.
- [37] R.T. Sibatov and D.V. Uchaikin, Fractional relaxation and wave equations for dielectrics characterized by the Havriliak-Negami response function, *arXiv preprint arXiv:1008.3972*.
- [38] E.C. Rosa and E.C. de Oliveira, Relaxation equations: Fractional models, *arXiv preprint arXiv:1510.01681*.
- [39] M.C. Tripathy, D. Mondal, K. Biswas, and S. Sen, Experimental studies on realization of fractional inductors and fractional order bandpass filters, *International Journal of Circuit Theory and Applications* 43 (9) (2015) 1183–1196.
- [40] J.T. Machado, Fractional generalization of memristor and higher order elements, *Communications in Nonlinear Science and Numerical Simulation* 18 (2) (2013) 264–275.
- [41] K. Biswas, G. Bohannan, R. Caponetto, A. Lopes, and T. Machado, *Fractional Order Devices*, Springer, 2017.
- [42] Y.-F. Pu, Measurement units and physical dimensions of fractance-part II: Fractional-order measurement units and physical dimensions of fractance and rules for factors in series and parallel, *IEEE Access* 4 (2016) 3398–3416.
- [43] A.M. Lopes and J.T. Machado, Modeling vegetable fractals by means of fractional-order equations, *Journal of Vibration and Control* 22 (8) (2016) 2100–2108.
- [44] D. El Khaled, N. Castellano, J. Gazquez, R.G. Salvador, and F. Manzano-Agugliaro, Cleaner quality control system using bioimpedance methods: A review for fruits and vegetables, *Journal of Cleaner Production* 140 (2017) 1749–1762.
- [45] Á. Kertész, Z. Hlaváčová, E. Vozáry, and L. Staroňová, Relationship between moisture content and electrical impedance of carrot slices during drying, *International Agrophysics* 29 (1) (2015) 61–66.
- [46] T.J. Freeborn, A.S. Elwakil, and B. Maundy, Compact wide frequency range fractional-order models of human body impedance against contact currents, *Mathematical Problems in Engineering* 2016.
- [47] F. Groeber, L. Engelhardt, S. Egger, H. Werthmann, M. Monaghan, and H. Walles, J. Hansmann, Impedance spectroscopy for the non-destructive evaluation of in vitro epidermal models, *Pharmaceutical Research* 32 (5) (2015) 1845–1854.
- [48] A. Tenreiro, et al., On the fractional-order modeling of wine, *European food research & technology*.
- [49] A.M. Lopes, J.T. Machado, E. Ramalho, and V. Silva, Milk characterization using electrical impedance spectroscopy and fractional models, *Food Analytical Methods* (2017) 1–12.
- [50] A.R. West, D.C. Sinclair, and N. Hirose, Characterization of electrical materials, especially ferroelectrics, by impedance spectroscopy, *Journal of Electroceramics* 1 (1) (1997) 65–71.
- [51] S. Ghasemi, M.T. Darestani, Z. Abdollahi, and V.G. Gomes, Online monitoring of emulsion polymerization using electrical impedance spectroscopy, *Polymer International* 64 (1) (2015) 66–75.
- [52] M. Glatthaar, M. Riede, N. Keegan, K. Sylvester-Hvid, B. Zimmermann, M. Niggemann, A. Hinsch, and A. Gombert, Efficiency limiting factors of organic bulk heterojunction solar cells identified by electrical impedance spectroscopy, *Solar Energy Materials and Solar Cells* 91 (5) (2007) 390–393.
- [53] M. Adachi, M. Sakamoto, J. Jiu, Y. Ogata, and S. Isoda, Determination of parameters of electron transport in dye-sensitized solar cells using electrochemical impedance spectroscopy, *The Journal of Physical Chemistry B* 110 (28) (2006) 13872–13880.
- [54] M. Grossi and B. Riccò, Electrical impedance spectroscopy (EIS) for biological analysis and food characterization: A review, *Journal of Sensors and Sensor Systems* 6 (2) (2017) 303–325.
- [55] T.K. Bera, Bioelectrical impedance methods for noninvasive health monitoring: *A review*, *Journal of Medical Engineering* 2014.
- [56] T.K. Bera, N. Jampana, and G. Lubineau, A LabVIEW-based electrical bioimpedance spectroscopic data interpreter (LEBISDI) for biological tissue impedance analysis and equivalent circuit modelling, *Journal of Electrical Bioimpedance*.
- [57] F. Seoane, J. Ferreira, J.J. Sánchez, and R. Bragós, An analog frontend enables electrical impedance spectroscopy system on-chip for biomedical applications, *Physiological Measurement* 29 (6) (2008) 267–278.
- [58] S. Guinta, Ask the applications engineer—resistors, *Analog Dialogue: A forum for the exchange of circuits, systems and software for real-world signal processing* 31 (1) (1997) 1–24.
- [59] F.B. Duarte and J.T. Machado, Describing function of two masses with backlash, *Nonlinear Dynamics* 56 (4) (2009) 409–413.